Thionation enhances the performance of polymeric dopant-free hole-transporting materials for perovskite solar cells

Haichang Zhang,[†] Maning Liu,[†] Wenjun Yang, Lauri Judin, Terttu I. Hukka, Arri Priimagi, Zhifeng Deng, Paola Vivo**

Dr. M. Liu, L. Judin, Dr. T. I. Hukka, Prof. A. Priimagi, Dr. P. Vivo
Faculty of Engineering and Natural Sciences, Tampere University, P.O. Box 541, FI-33014 Tampere, Finland
E-mail: paola.vivo@tuni.fi

Dr. H. Zhang, Dr. Z. Deng
National and Local Joint Engineering Laboratory for Slag Comprehensive Utilization and Environmental Technology, School of Material Science and Engineering, Shanxi University of Technology, Hanzhong 723001, PR China
E-mail: dengzf@snut.edu.cn

Dr. W. Yang
Key Laboratory of Rubber-Plastics of Ministry of Education/Shandong Province (QUST), School of Polymer Science & Engineering, Qingdao University of Science & Technology, 53-Zhengzhou Road, Qingdao, 266042, China

[†]H. Zhang and M. Liu contributed equally to this work

Keywords: dopant-free; hole-transporting materials; thionation; perovskite solar cells; diketopyrrolopyrrole

Abstract

To date, the most efficient perovskite solar cells (PSCs) require hole transporting materials (HTMs) that are doped with hygroscopic additives to improve their performance. Unfortunately, such dopants negatively impact the overall PSCs stability and add cost and complexity to the device fabrication. Hence, there is a need to investigate new strategies to boost the typically modest performance of dopant-free HTMs for efficient and stable PSCs. Thionation is a simple and single-step approach to enhance the carrier-transport capability of organic semiconductors, yet still completely unexplored in the context of HTMs for PSCs. In this work, a novel polymeric semiconductor, **P1**, based on diketopyrrolopyrrole (DPP) moiety, is proposed as dopant-free HTM. Its modest performance in PSCs (PCE = 7.1%) is significantly enhanced upon thionation of the DPP moiety. The resulting dithioketopyrrolopyrrole (DTPP)-based HTM, **P2**, leads to PSCs with nearly 40%

performance improvement (PCE = 9.7%) compared to devices based on the non-thionated HTM (**P1**). Furthermore, thionation also remarkably boosts the shelf-storage and thermal stability with respect to traditional spiro-OMeTAD-based PSCs. This work provides useful insights to further design effective dopant-free HTMs employing the straightforward one-step thionation strategy for efficient and stable PSCs.

1. Introduction

Power conversion efficiency (PCE) and stability of perovskite solar cells (PSCs) are heavily dependent on the adopted hole-transporting materials (HTMs), which form the key working junction with the perovskite in the solar cell.[1] To date, nearly all the most efficient PSCs employ organic HTMs, with 2,2',7,7'-tetrakis(*N*,*N*-di-p-methoxyphenylamine)-9,9'-spirobifluorene (spiro-OMeTAD) being the most popular choice. However, spiro-OMeTAD is not suitable for large-scale development of PSCs because of its onerous multistep synthesis and demanding purification.[2] Furthermore, its inadequate hole mobility and conductivity require the addition of chemical p-dopants to ensure the PSCs to work efficiently.[2] Nevertheless, these hygroscopic additives negatively impact the device stability.[1] Hence, there is an urgent need to develop dopant-free HTMs with good charge transport characteristics in pristine form to ensure efficient charge extraction and high PSCs stability at the same time.[3][4] To this aim, a fairly rich variety of dopant-free molecular HTMs has been already proposed,[3] with those based on anthanthrone,[5][6] triazatruxene,[7] spiro-fluorene,[8] or tetra-thiafulvalene[9] moieties being the most promising ones. Significantly less examples of dopant-free polymeric HTMs can be found in literature, mostly obtained from the costly benzodithiophene (BDT) or monofluoro-substituted benzothiadiazole (FBT) units via challenging synthesis procedures.[10] Solution processable diketopyrrolopyrrole (DPP)-based polymers display high charge carrier mobility ranging from 0.1 to 10 $cm^2\ V^{-1}\ s^{-1}$, because of the strong π- π stacking between the conjugated backbones.[11] They have been widely used in organic field-effect transistors (OFETs)[12][13,14] and organic photovoltaics (OPVs),[15][16] and

they could be ideal candidates when aiming at cheaper dopant-free polymeric HTMs for PSCs. However, while their energy levels are well aligned with the valence band (VB) and conduction band (CB) of perovskite, on the other hand only few examples of DPP-based PSCs have been reported in the literature and their efficiency remains modest.[17–19] Hence, strategies are needed to harness the full potential of this facile class of polymers.

Thionation is a straightforward oxygen-sulfur atomic substitution that remarkably tunes the material's optical and electronic properties without the need to synthesize a new compound from scratch but via a simple and single-step reaction.[20–25] Seferos and coworkers demonstrated that perylene diimide small molecules display enhanced charge transport characteristics upon thionation, because of the change in their morphological and photophysical properties.[24] Tieke et al. reported about the thionation of DPP-polymers to synthesize the corresponding dithioketopyrrolopyrrole (DTPP) derivatives with low bandgap and broad absorption using Lawesson's reagent.[26] More recently, Zhang et al. demonstrated that isomeric DTPP polymers could be promising building blocks for OFETs, with hole mobility up to 0.49 $cm^2 V^{-1} s^{-1}$.[27] In addition, this work showed that the Highest Occupied Molecular Orbital (HOMO) levels of the material could be increased upon thionation. Both the high hole mobility and high HOMO level are essential prerequisites when designing dopant-free HTMs for PSCs. While thionation has been very recently employed to tune the properties of n-type materials in OPVs,[20] to the best of our knowledge this strategy remains still completely unexplored in the context of HTMs for PSCs applications.

In this work, we show that the thionation of a novel donor (D)-acceptor (A) polymer (**P1**) with π-electron rich indacenodithiophene (IDT) and π-electron deficient diketopyrrolopyrrole (DPP) moieties can significantly increase the figure of merit of PSCs employing DPP-based polymeric HTMs without dopants. In fact, **P2**-based PSCs show a nearly 40% device performance improvement (PCE = 9.7%) compared to **P1**-based ones (PCE = 7.1%). We attribute such an enhancement to the role of thionation in effectively improving the interfacial

hole transfer dynamics, as demonstrated by our combined electrochemical, computational, and photophysics studies. Finally, the stability of PSCs employing **P1** or **P2** outperforms that of devices based on the traditional spiro-OMeTAD HTM, as expected thanks to the lack of hygroscopic additives in **P1** and **P2** and to their remarkable thermal stability.

2. Results and Discussion

2.1 Design and synthesis

Two π-conjugated polymers with D-A structures, **P1** and **P2**, were synthesized starting from electron-donating dibromo-IDT and electron-withdrawing di(trimethylstannyl)-substituted DPP monomers. Small molecules or polymers with an alternating D-A structure have demonstrated high performance in organic electronics due to their narrow band gaps and effective intramolecular charge transfer capability.[28–32] Particularly, we selected IDT being an interesting electron-rich moiety derived from thiophene with a fully planar core, extended π-conjugation, and high electronic density arising from a large fused system.[33]Moreover, the multiple available positions for substitutions in IDT guarantee good solubility and wide range fine-tuning of the polymers energy levels.[34] DPP is a versatile unit with short π-π stacking distance and highly coplanar polymer chains that result into excellent charge mobility.[35]

In our design, we co-polymerized the electron-deficient DPP-based monomer with dibromo-IDT *via* palladium-catalyzed Stille coupling to yield the target material **P1** (**Scheme 1**). Both DPP- and IDT-based monomers are commercially available and were purchased from Derthon Optoelectronic Materials Science Technology Co LTD. In order to probe the beneficial role of thionation on polymeric HTMs for PSCs, we synthesized another polymer (**P2**), where the oxygen atom of the DPP core was replaced by sulfur yielding a DTPP-based material (**P2**), by treating **P1** solution with Lawesson's reagent (2,4-bis(4-methoxyphenyl)-1,3,2,4-dithiadi-phosphetane-2,4-disulfide) (Scheme 1). Further details on the synthesis of **P1** and **P2** can be found in the Supporting Information.

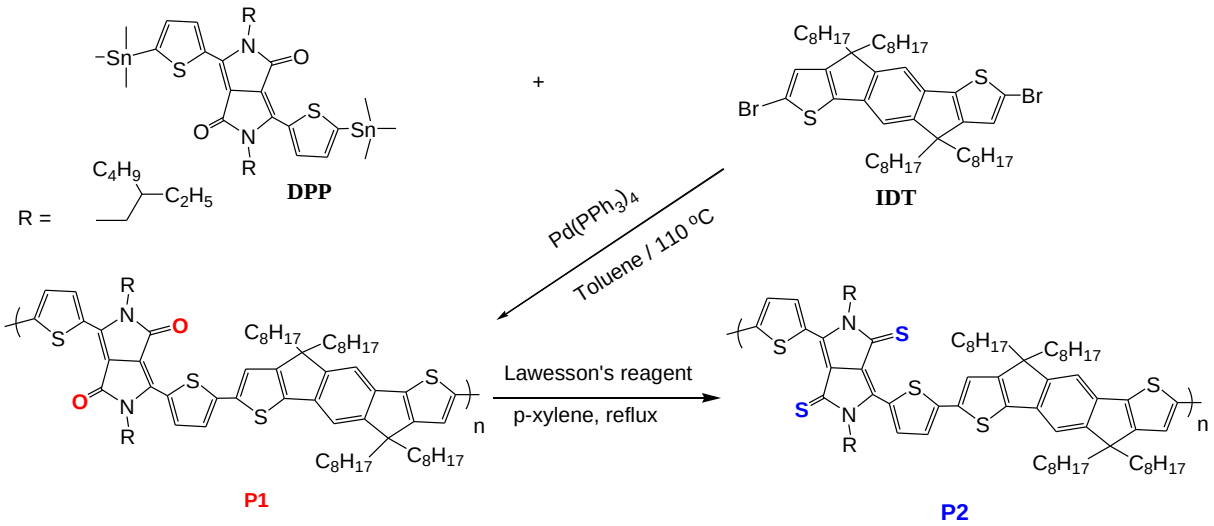

Scheme 1. Synthetic route for **P1** and **P2** polymers.

The weight-average molecular weights (M_w) of the polymers **P1** and **P2**, determined by gel permeation chromatography (GPC, Figure S1), lie between 82 kDa and 84 kDa and the dispersity index in the range 2.8–4.0. The polymer structures were analyzed by FTIR and ^{1}H-NMR spectroscopy (see Supporting Information for further details and Figures S2–S5). The FTIR data (**Figure 1**) clearly prove the thiocarbonylation reaction, which alters the O atom from DPP core into S atom, as the absorption peak between 1622 and 1758 cm^{-1} (C=O stretching of DPP core, dark green band) disappears after thionation, and a new band, attributed to the C=S stretching vibration, emerges at 1140 cm^{-1}.[26,27] Proton spectra of the polymers are shown in Figures S6–S8. The spectra contain all the expected signals to confirm the corresponding molecular structures of **P1** and **P2**. The signals between 0.7 and 2.09 ppm originate from the alkyl groups, while the chemical shift between 6.99 and 8.94 ppm are ascribed to the DPP and IDT core, respectively. After thionation, the signals from DPP with chemical shift of 7.38 ppm can be found at 7.36 ppm (DTPP, Figure S8).

The thermal stability of the polymers was investigated with thermogravimetric analysis (TGA) and differential scanning calorimetry (DSC). Experimental details, together with TGA and DSC curves, can be found in the Supporting Information. From TGA analysis, the decomposition temperatures (T_d), corresponding to 5 % weight loss of **P1** and **P2**, are 380 °C

and 367 °C, respectively (Figure S9). In other words, both the polymers exhibit a good thermal stability, comparable to that of other high-performing polymeric dopant-free HTMs,[36–38] and well above solar cell operational conditions. From DSC data, no distinct glass transition temperature (T_g) can be identified between 30 °C and 270 °C (Figure S10). This is in line with what has been reported for other DPP-based polymers,[39] and it is related to the high rigidity of the polymer backbone as well as to the strong intermolecular interactions between the neighboring polymer chains. This, in turn, confirms that **P1** and **P2** are morphologically stable, with no phase transitions between 30 °C and 270 °C. In comparison, for the most widely adopted HTM, spiro-OMeTAD, the T_g is relatively low (125 °C).[40] These results suggest that **P1**/**P2** could have a positive impact on the thermal stability of resultant PSCs compared to standard spiro-OMETAD-based devices, as will be demonstrated in Section 2.6.

2.2 Optical and electrochemical characterization

The absorption spectra of **P1** and **P2** in chloroform (c= 0.05 g/L) and in solid state (thin spin-coated films) are shown in **Figure 2**. The corresponding optical data are summarized in Table 1. Both polymers exhibit broad optical absorption between 500 and 830 nm with strong absorption peaks at 712 nm (**P1**) and 719 nm (**P2**) in solution (Figure 2). In solid state, the absorption extends up to the near-infrared (NIR) region, with absorption maximum at 721 nm (**P1**) / 738 nm (**P2**) and a long-wavelength tail reaching to 1000 nm. The absorption in the NIR region indicates a highly conjugated backbone and/or efficient molecular packing in the thin film state.[27] The solid-state spectra of **P1** and **P2** are bathochromically (red) shifted by 9 and 19 nm, respectively, compared to the solution spectra (Figure 2, Figure S11). This could be due to the strong packing and π-π interactions in thin films, induced by the closer distance between the polymer backbones compared to solution phase. These interactions are beneficial for the charge transport between neighboring molecules, which potentially promote charge mobility and their conductivity, too.[41,42]

When we compare the spectra of the non-thionated **P1** with those of the thionated **P2**, a small bathochromic shift in the absorption maxima is observed (7 nm shift in solution spectra and 17 nm in thin film spectra, Figure 2, Table 1). The shift toward longer wavelengths might be due to the stronger electron-withdrawing ability of DTPP unit with respect to DPP,[43] which induces strong D-A stacking interaction in **P2**'s backbone structure, thus eventually promoting the charge transfer within the individual molecule.

When designing novel HTMs for PSCs, it is essential to tune their energy levels in order to match the VB and CB of perovskite. This ensures effective hole extraction from the perovskite layer and meanwhile prevents electrons from reaching the top-electrode (e.g. Au). We conducted cyclic voltammetry (CV) measurements to determine the HOMO/LUMO energy levels of the **P1** and **P2** films. Details on the CV measurements and the voltammograms are given in Supporting Information (Figure S12). The polymers exhibit two reversible cathodic waves and quasi-reversible anodic curves. From the oxidation and reduction onset potentials, the derived HOMO/LUMO energy levels are -5.44 eV/-3.66 eV and -5.23 eV/-3.79 eV for **P1** and **P2**, respectively. These results are visually summarized in **Scheme 2**, together with the energy levels of perovskite and of all the other constituents of the PSCs architecture studied in this work. The energy levels of both polymers are well aligned to perovskite VB and CB, indicating the suitability of **P1** and **P2** as HTMs. In fact, Murata et al. have identified the selection criteria in terms of energy levels for HTMs, showing that the HTM HOMO and LUMO levels should be at least 0.1 and 0.25 eV higher than the perovskite VB and CB, respectively.[44] Both P1 and P2 fulfill this requirement, indicating that they can potentially realize efficient hole injection while effectively blocking electrons. Furthermore, the DTPP-based polymer **P2** has higher HOMO (0.21 eV increase) and lower LUMO (0.13 eV decrease) levels than the corresponding non-thionated **P1**. The increase of the HOMO level upon thionation, already demonstrated by Zhang et al.,[27] further improves the energetic alignment of **P2** with the perovskite layer, suggesting a better-performing HTM in PSCs

compared to the DPP-based one (**P1**). Furthermore, the simultaneous lowering of LUMO level in **P2** contributes to narrowing the material's bandgap, hence enhancing the light harvesting in the NIR.

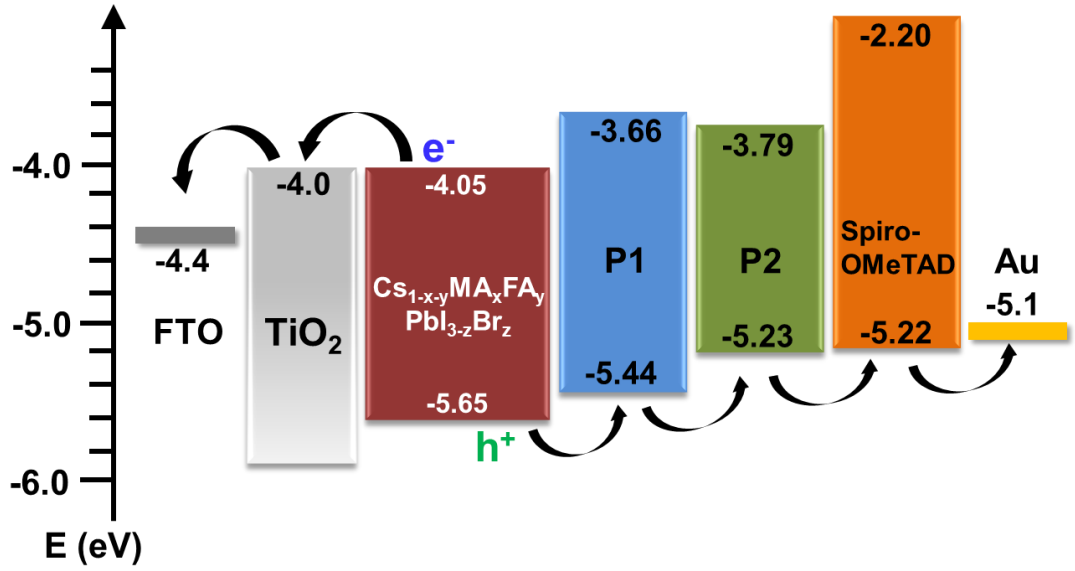

Scheme 2. Energy level diagram of polymers **P1**, **P2**, and spiro-OMeTAD and of the other layers of the PSCs considered in this study. Particularly, we have adopted a triple cation $Cs_{1-x-y}MA_xFA_yPbI_{3-z}Br_z$ perovskite light absorber. The energy levels of each material (except those of the new HTMs) have been taken from literature.[45–47]

The effect of thionation on the polymers' ground state frontier molecular orbitals (FMO), electron density distributions, as well as the highest occupied molecular orbital (HOMO) and the lowest unoccupied molecular orbital (LUMO) energy levels were investigated further computationally via density functional theory (DFT) at the M062X/6-31G(d,p) level using the Gaussian 09 program package. Two constitutional repeating units (CRU) long (n=2) molecules, i.e. dimers, with methyl groups as the substituents R (Scheme 1) were used as models. For the ground state structures of the dimers, see Figure S13 in Supporting Information. Figure S14 shows that the DPP-based polymer **P1** exhibits a DPP-dominating LUMO distribution with some of the electron wave function delocalized at the IDT unit, while the electron distribution of the LUMO for the thionated polymer **P2** localizes only on the electron-withdrawing DTPP core. The difference between the polymers' LUMO electron

densities could be due to DTPP with a stronger electron-acceptor ability compared to DPP. The HOMO orbitals of both polymers are similar, as the electron wave functions are mainly delocalized along the polymer backbone. When the polymers are excited, electron transfer takes place from the conjugated backbone to the DPP or DTPP unit. Quantum computation results also indicate that the thionation reaction could increase the HOMO energy levels and reduce the LUMO energy levels of the polymers, which is in good agreement with the electrochemical results. The HOMO/LUMO energy levels and the HOMO–LUMO gaps of the polymers predicted via the DFT calculations are different from the electrochemical ones. This is ascribed to the fact that the DFT calculations were carried out with dimer models instead of full polymers, and the intermolecular interaction was not taken into account. We will address the intermolecular interaction below and present the bulk hole mobilities of the HT-materials calculated according to the hopping model[48] with DFT using two CRUs (with n=1) sliding on top of each other (for the details of the computational procedure, see Supporting Information). Figure S13 shows that the backbone of the DTPP-polymer is more planar than that of the DPP-polymer. Planarity is beneficial for both the intra- and intermolecular charge transfer.

2.3 Thionation-enhanced hole mobility

We computed the bulk hole mobilities for **P1** and **P2** with DFT to gain understanding on their material characteristics (see Supporting Information for the details). Furthermore, in order to a) obtain experimental reference values for the hole mobilities in a device and to b) demonstrate the suitability of these isomeric DTPP polymers as building blocks for OFETs, we explored the charge transport characteristics of **P1** and **P2** by fabricating and analyzing bottom gate/bottom contact field effect transistors. Figure S15 and Figure S16 show the transfer and output characteristics of the OFETs (for the corresponding device performance data see Table S1). Both polymers exhibit p-type behavior. The measured OFET hole mobility of the DPP-polymer is up to 1.02 $cm^2 V^{-1} s^{-1}$ (**P1**). After the thionation reaction, the

OFET hole mobility increased significantly to as high as 1.64 $cm^2\ V^{-1}\ s^{-1}$ for **P2**. The bulk mobility values of 1.7×10^{-3} and 8.8×10^{-3} $cm^2\ V^{-1}\ s^{-1}$ calculated with DFT for **P1** and **P2**, respectively, are in accordance with the experimental trend and typical for hole mobility values of DPP-based materials.[49,50] The notable enhancement of both experimental OFET and computed bulk hole mobility of the thionated-polymer could be ascribed to the following reasons: *(i)* in the thin film state, the slightly stronger intermolecular interactions of the DTPP-based polymer compared to the DPP-based polymer (revealed by bathochromic shift from solution to thin film) is helpful for the hole transfer between the neighboring molecules; *(ii)* the more planar polymer backbone and stronger D–A effect in the DTPP-polymer is advantageous for the intra- and intermolecular hole transfer.

2.4 Photovoltaic performance

To study the effect of thionation of HTM on the performance of PSCs, **P1** and **P2** were incorporated without any doping additives in standard mesoporous *n-i-p* structures. The devices consisted of a triple cation (Cesium (Cs), methylammonium (MA), and formamidinium (FA)) $Cs_{1-x-y}MA_xFA_yPbI_{3-z}Br_z$ perovskite layer on a fluorine-doped tin oxide (FTO)/TiO_2 compact layer (c-TiO_2)/TiO_2 mesoporous layer (m-TiO_2) substrate, fabricated by one-step deposition method (see the detailed procedure in Supporting Information). The full PSC structure is FTO/c-TiO_2/m-TiO_2/$Cs_{1-x-y}MA_xFA_yPbI_{3-z}Br_z$/HTM (**P1** or **P2**)/Au, as illustrated in **Figure 3**a. Additionally, PSCs with standard spiro-OMeTAD HTM (with and without dopants) were fabricated for comparison under identical experimental conditions. The thicknesses of each PSCs layer, derived from cross-sectional scanning electron microscopy (SEM) image (Figure S18a), are in line with those reported in previous studies.[51] For both **P1** and **P2**, a thickness of nearly 135 nm (films spin-coated from chlorobenzene solution with c = 10 mg/mL) was used (Figure S18b).

The current density (*J*) –voltage (*V*) curves of the best-performing (champion) devices based on the different HTMs, recorded under standard 1 Sun condition (100 mW cm^{-2} AM 1.5 G

illumination), are depicted in Figure 3b and Figure S19. The averaged photovoltaic performance (20 devices per HTM) along with the standard deviation, together with the photovoltaic parameters of the champion cells (derived from Figure 3b), are summarized in **Table 2**. The high reproducibility of our results is demonstrated by the small standard deviations.

The DTPP-based HTM **P2** leads to PSCs with a remarkable 37% performance improvement (average PCE = 9.7%) compared to devices based on the non-thionated **P1** (Table 2). The improvement in the PCE is determined by the increase in both short-circuit current density (J_{SC}) and fill factor (*FF*). The J_{SC} enhancement is related to the beneficial effect of thionation on the hole injection process from perovskite to HTM, as discussed in detail in the next section. To clarify the reasons for the enhanced *FF*, we have extracted the series (R_S) and shunt (R_{SH}) resistance of the devices, according to the 1-diode model,[52] from the *J*– *V* curves in a backward scan (Table 2). Both R_{SH} and R_S affect the *FF*, with lower R_S and higher R_{SH} being needed for enhancing the FF values.[53] Data in Table 2 confirm this trend since **P2** cells have lower R_S and higher R_{SH} (nearly 1 order of magnitude) than the **P1**-based cells. As observed in earlier reports, a low *FF* is an indicator of low mobility and conductivity of the material.[36,38] The intermolecular charge transport is enhanced upon thionation, as demonstrated in Section 2.3, thus explaining the increase in the *FF* of the corresponding DTPP-based photovoltaic devices. In addition, it is reported that *FF* is also influenced by non-geminate charge recombination at the perovskite interface,[63] thus, the improved FF obtained by **P2**-based cells suggests that thionated **P2** could more effectively hinder the interfacial charge recombination compared to **P1**, which will be evidenced in the time-resolved photoluminescence study reported in next section.

It is worth noting that **P1**- and **P2**-based devices presented nearly identical V_{OC} values. This confirms that in perovskite solar cells the V_{OC} is mainly determined by the bulk and surface recombination in the perovskite, while being less sensitive to the energetic offset between the

VB of the perovskite and the HOMO level of the HTMs, as recently reported by Dänekamp et al.[54]

Control devices based on the doped Spiro-OMeTAD HTM lead to an increased PCE, yet comparable, with respect to **P1**/**P2**-based solar cells. In order to understand the poorer performance of **P1** and **P2** HTMs in perovskite solar cells with respect to the spiro-OMeTAD, the morphology of their thin films deposited on perovskite-coated glass substrates has been investigated by atomic force microscopy (AFM), as shown in Figure S17. The surface root mean square roughness values for both **P1** and **P2** films were similarly above 20 nm, which are over two times higher than the roughness of spiro-OMeTAD film (~ 9 nm) deposited on perovskite. Smoother spiro-OMeTAD film on top of the perovskite layer could be more favorable for efficient hole transfer compared to **P1** or **P2** film (as demonstrated in following Section), and this could also partly explain the enhanced device performance of spiro-OMeTAD based cells. In case of **P2** film, we also note larger domain size compared to **P1** films (Figure S17), due to the thionation-induced phase aggregation which could reduce pin holes and improve the hole transfer.

The lower performance of PSCs employing **P1** or **P2** is compensated by the lack of additives, which will have a beneficial effect on the device stability (see Section 2.6). In fact, if all the HTMs are used without dopants, a huge enhancement of **P1** and **P2** performance with respect to Spiro-OMeTAD is observed (Table 2). Furthermore, **P1** and **P2** are significantly cheaper than Spiro-OMeTAD (see cost analysis in Supporting Information), and the lack of dopants additionally reduces the cost and complexity of device fabrication. Finally, it is worth emphasizing that, while for spiro-OMeTAD optimal thickness values are well known and adopted in this work as well, for **P1** or **P2** HTMs we have not yet optimized their layer thicknesses in PSCs, which could potentially lead to even better performance of the corresponding devices.

From the *J– V* curves in forward and backward scans (Figure S18), we note that both **P1**- and **P2**-based cells display significantly lower hysteresis than spiro-OMeTAD-based devices. It is well known that the carrier transfer dynamics at the interfaces in PSCs (including the perovskite|HTM interface) affect the overall device hysteresis.[55] Lower hysteresis can thus partly attributed to a better interaction between perovskite and **P1** or **P2**, most likely promoted by the presence of S atoms that coordinate to Pb of perovskite, as observed by Zheng et al. in case of thiolated HTMs.[56,57]

2.5 Influence of thionation on the interfacial hole transfer process

When aiming at highly efficient PSCs, it is crucial to probe the hole injection dynamics at the perovskite/HTM interface.[58] In fact, it has been recently reported that a swift hole injection dominates the overall charge separation efficiency with respect to a relatively slow electron injection.[47,59]

To evaluate the hole-injection process from the perovskite VB to the HOMO level of the HTMs (**P1** and **P2**), steady-state photoluminescence (PL) experiments (details in Supporting Information) on glass/perovskite and glass/perovskite/HTM samples were conducted. **Figure 4**a shows the stronger PL quenching capability of **P2** with respect to the non-thionated **P1**, although the reference spiro-OMeTAD sample displays the strongest quenching effect. The calculated quenching efficiencies, or in other words the hole-injection yields, are 77.9 % and 96.2 % for **P1** and **P2**, respectively. The remarkable hole-injection yield increase achieved when **P2** is employed, suggests that thionation promotes the extraction of the photogenerated holes from the perovskite layer at the perovskite/**P2** interface. This could partly explain the higher J_{SC} in **P2**-based solar cells with respect to **P1**-based ones (Table 2).

To assess the influence of thionation on the hole transfer dynamics, we monitored the time-resolved PL decays on glass/perovskite and glass/perovskite/HTMs samples by time-correlated single photon counting (TCSPC) measurements (experimental details in Supporting Information). The PL decays are presented in Figure 4b. The excitation wavelength of 648 nm

was selected not to excite the residual PbI_2 (~550 nm) potentially present in the perovskite layer.[60] The PL decay of pristine perovskite film shows the perovskite excited state decay with relatively long effective lifetime (370.9 ns), similarly as in previous works.[61] A clear acceleration of the PL decay is observed for glass/perovskite/**P1** sample, thus indicating that hole transfer from the perovskite to **P1** occurs at the interface. An even more pronounced acceleration is detected for glass/perovskite/**P2**, hence suggesting that the hole transfer from perovskite to **P2** is significantly faster than that to **P1**. On the other hand, the glass/perovskite/spiro-OMeTAD reference sample shows the most accelerated PL decay compared to **P1** or **P2**, indicating that a hole injects from perovskite to spiro-OMeTAD in the most efficient way, which is consistent with the corresponding solar cells results presented in previous section.

In order to quantitatively assess the influence of thionation reaction on hole transfer process, we now focus only on **P1** and **P2**. All PL decays can be well fitted with bi-exponential decay model (details in Supporting Information). The first component is attributed to the radiative charge recombination related to carrier trap states, while the second component is linked to the non-geminate free carrier (electron and hole) recombination and hole injection process.[47,62] The results of the fitting (**Table 3**) reveal that both HTMs display similar decay lifetimes of the first component, with τ_1 being 7.2 ns and 6.5 ns for **P1** and **P2** samples, respectively. However, the first component shows much higher initial amplitude (A_1 > 50 %) for **P2** PL decay with respect to the corresponding initial amplitude (A_1 < 10 %) of **P1** containing sample (Table 3), indicating that the surface states of perovskite in **P2**-based sample could be effectively passivated upon the thionation reaction compared to the non-thionated **P1**-based sample. In addition, the decay lifetime τ_2 of the second component of **P2**-based sample (38.3 ns) is much shorter than that of the sample containing **P1** (98.6 ns). Such an acceleration in the lifetime of the second component suggests that, by the replacement of oxygen with sulfur atoms upon thionation, the properties of the perovskite|HTM interface can

be effectively modified, hence leading to suppressed charge recombination and promoted swift hole injection. Our results clarify, for the first time, the role of thionation in the charge (hole) transfer dynamics: thionation affects both the trap-state-mediated recombination, the non-geminate charge recombination, and the hole injection reaction.

Hole injection rate and yield can be also estimated by comparing the lifetimes of the observed PL decays (see the analysis method in Supporting Information).[63] Interestingly, the hole injection rate ($\tau_{h\text{-}inj}$) of **P2** (17.7 ns) is significantly faster than that of **P1** (113.8 ns) by nearly one order of magnitude, confirming that thionation promotes a fast hole-injection at the interface between perovskite and **P2**. The estimated hole injection rate for **P2** in nanosecond timescale is still slower than values reported using femtosecond transient absorption and terahertz spectroscopies (from 200 fs to several tens of picoseconds).[45] This difference could be due to the multi-phasic hole injection processes, i.e. more than 3 components over fs-ns time scales, which have been recently reported. The hole injection yields for **P1** and **P2** were estimated by using Equation S2-S4 (Supporting Information). Upon thionation, the hole injection yield ($\Phi_{h\text{-}inj}$) of **P2** exceeds 95 % (Table 3), while that of non-thionated **P1** is limited to less than 80 %, in a good agreement with the quenching efficiency data of the steady-state PL spectra (Figure 4a).

2.6 Stability

The stability of non-encapsulated PSCs employing the dopant-free polymeric HTMs **P1**/**P2** was studied by analyzing the PCE decay curves for the devices in shelf-storage conditions (darkness, dry environment with RH ~10%). Identical experiments were conducted in parallel on doped spiro-OMeTAD PSCs. The normalized PCE of the 3 champion cells containing **P1**, **P2**, or spiro-OMeTAD as a function of time are presented in **Figure 5**a. Additionally, equivalent degradation studies were conducted on several devices per each PSC structure, and a similar degradation pattern as the one in Figure 5a was confirmed. **P2**-based cell exhibit remarkably improved stability compared to **P1**-based cell, sustaining 70% and 49% of the

initial PCE, respectively, after nearly 100 days of storage. Doped spiro-OMeTAD cells instead decrease their performance more quickly (29% of their original PCE retained in nearly 100 days under identical experimental conditions). This is expected since neither **P1** nor **P2** contain hygroscopic dopants that, in case of spiro-OMeTAD, can cause moisture intrusion in the perovskite layer with a detrimental effect on device degradation. This effect would be even more evident when storing the devices in high-humidity atmosphere, as demonstrated in Ref .[64]

P2-based PSCs show the slowest degradation in air. In order to identify the reasons for the difference in degradation kinetics between **P1**-, **P2**-, or spiro-OMeTAD-cells, we have measured the water contact angles on the perovskite/HTM films (Figure S19). The contact angle values are $103.26^{o} \pm 0.39^{o}$, $109.75^{o} \pm 1.13^{o}$, $66.82^{o} \pm 0.59^{o}$ for **P1**, **P2**, and doped spiro-OMeTAD, respectively. These results indicate that **P2** is the most hydrophobic material, since it displays higher moisture resistance. Being able to keep perovskite more protected from moisture, **P2** allows enhanced PSC stability.

Finally, PSCs based on **P1**, **P2**, or spiro-OMeTAD HTMs underwent a straightforward high-temperature stability test as in Ref. [36], in order to evaluate the thermal stability of the devices. The normalized PCEs of the solar cells, before and after being heated at 65 ℃ for 12 h in nitrogen atmosphere, are reported in Figure 5b. The devices employing the new polymeric HTMs, and **P2** in particular, retain the initial performance much better than those with the traditional spiro-OMeTAD. The high thermal stability of these polymers, already suggested by the results of the DSC characterization (Section 2.1), indicates their potential use for stable PSCs. **P2** displays the highest thermal stability, with practically no change in the performance after 12h of heating. Thionation increases the number of S atoms in **P2** HTM with respect to P1, in turn potentially promoting Pb-S coordination bonding, as already mentioned. Since Pb-S bond shows higher exciton binding energy than Pb-O bond, [65,66] thionation may lead to

higher heating tolerance for perovskite or, in other words, higher thermal stability of the corresponding device.

3. Conclusions

In conclusion, we propose thionation as an effective and straightforward strategy to dramatically boost the performance of dopant-free polymeric hole-transporting materials for perovskite solar cells. Thionation of a novel donor (D)-acceptor (A) polymer (**P1**) with π-electron rich indacenodithiophene (IDT) and π-electron deficient diketopyrrolopyrrole (DPP) moieties (leading to polymer **P2**) enhances the power conversion efficiency of the corresponding solar cell devices by nearly 40%. We attribute such an increase to the role of thionation in effectively improving both the hole transport within the HTM (bulk hole mobility increased by 5 times upon thionation) and the interfacial hole transfer dynamics. The latter results mainly from three factors: 1) thionation increases the HOMO level of **P2** (210 meV higher HOMO than **P1**), providing more driving force (i.e. Gibbs free energy) for the hole injection from perovskite VB to the HTM's HOMO; 2) The coordination Pb-S bonds promoted by the increasing number of S atoms of the thionated HTM (**P2**) may also potentially guarantee an effective pathway for swift and efficient hole injection; 3) thionation can effectively passivate the surface states of perovskite film, i.e. diminish the deep trap states, which is beneficial for fast hole injection at the perovskite interface.

Finally, the stability of PSCs employing **P1** or **P2** outperforms that of devices based on the traditional spiro-OMeTAD HTM, as expected due to the lack of hygroscopic additives in **P1** and **P2** and to their remarkable thermal stability.

Supporting Information

Supporting Information is available from the Wiley Online Library or from the author.

Acknowledgements

We thank Mr. Hannu Pasanen for helping with SEM imaging, Mr. Lassi Sukki for helping with the water contact angle measurements, Mrs. Maiju Hiltunen and Mrs. Jenni Uotila for helping with AFM study.

P.V. and M.L. acknowledge Jane & Aatos Erkko foundation (project 'ASPIRE') for financial support. H.Z. and Z.D. acknowledge the support from the Natural Science Foundation of China, under Grant 21805151, and the Natural Science Foundation of Shandong Province, China, under Grant ZR2018MB024.This work is part of the Academy of Finland Flagship Programme. Photonics Research and Innovation (PREIN), decision number 320165.

Received: ((will be filled in by the editorial staff))
Revised: ((will be filled in by the editorial staff))
Published online: ((will be filled in by the editorial staff))

References

[1] A. Kumar Jena, A. Kulkarni, T. Miyasaka, Chem. Rev. **2019**, *119*, 3036.

[2] P. Vivo, J. Salunke, A. Priimagi, *Materials (Basel).* **2017**, *10*, 1087.

[3] Q. Wang, N. Phung, D. Di Girolamo, P. Vivo, A. Abate, *Energy Environ. Sci.* **2019**, *12*, 865.

[4] H. D. Pham, L. Xianqiang, W. Li, S. Manzhos, A. K. K. Kyaw, P. Sonar, *Energy Environ. Sci.* **2019**, *12*, 1177.

[5] H. D. Pham, T. T. Do, J. Kim, C. Charbonneau, S. Manzhos, K. Feron, W. C. Tsoi, J. R. Durrant, S. M. Jain, P. Sonar, *Adv. Energy Mater.* **2018**, *8*, 1703007.

[6] H. D. Pham, K. Hayasake, J. Kim, T. T. Do, H. Matsui, S. Manzhos, K. Feron, S. Tokito, T. Watson, W. C. Tsoi, N. Motta, J. R. Durrant, S. M. Jain, P. Sonar, *J. Mater. Chem. C* **2018**, *6*, 3699.

[7] K. Rakstys, A. Abate, M. I. Dar, P. Gao, V. Jankauskas, G. Jacopin, E. Kamarauskas, S. Kazim, S. Ahmad, M. Grätzel, M. K. Nazeeruddin, *J. Am. Chem. Soc.* **2015**, *137*, 16172.

[8] K. Liu, Y. Yao, J. Wang, L. Zhu, M. Sun, B. Ren, L. Xie, Y. Luo, Q. Meng, X. Zhan, Q. Meng, W. Lövenich, C. J. Brabec, M. Grätzel, A. Hagfeldt, *Mater. Chem. Front.* **2017**, *1*, 100.

[9] J. Liu, Y. Wu, C. Qin, X. Yang, T. Yasuda, A. Islam, K. Zhang, W. Peng, W. Chen, L. Han, *Energy Environ. Sci.* **2014**, *7*, 2963.

[10] W. Zhou, Z. Wen, P. Gao, *Adv. Energy Mater.* **2018**, *8*, 1702512.

[11] X. Guo, B. Zhang, Z. Lin, J. Su, Z. Yang, C. Zhang, J. Chang, S. (Frank) Liu, Y. Hao, *Sustain. Energy Fuels* **2018**, *2*, 2154.

[12] B. Lim, H. Sun, J. Lee, Y.-Y. Noh, *Sci. Rep.* **2017**, *7*, 164.

[13] T.-J. Ha, P. Sonar, A. Dodabalapur, *Appl. Phys. Lett.* **2011**, *98*, 253305.

[14] P. Sonar, J.-M. Zhuo, L.-H. Zhao, K.-M. Lim, J. Chen, A. J. Rondinone, S. P. Singh, L.-L. Chua, P. K. H. Ho, A. Dodabalapur, *J. Mater. Chem.* **2012**, *22*, 17284.

[15] W. Li, K. H. Hendriks, M. M. Wienk, R. A. J. Janssen, *Acc. Chem. Res.* **2016**, *49*, 78.

[16] Y. Li, P. Sonar, L. Murphy, W. Hong, *Energy Environ. Sci.* **2013**, *6*, 1684.

[17] Y. S. Kwon, J. Lim, H.-J. Yun, Y.-H. Kim, T. Park, *Energy Environ. Sci.* **2014**, *7*, 1454.

[18] A. Dubey, N. Adhikari, S. Venkatesan, S. Gu, D. Khatiwada, Q. Wang, L. Mohammad, M. Kumar, Q. Qiao, *Sol. Energy Mater. Sol. Cells* **2016**, *145*, 193.

[19] H. Maruo, Y. Sasaki, K. Harada, K. Suwa, K. Oyaizu, H. Segawa, K. Carter, H. Nishide, *Polym. J.* **2019**, *51*, 91.

[20] K. Rundel, Y. Shin, A. Sidney, R. Chesman, A. C. Y. Liu, A. Welford, L. Thomsen, M. Sommer, C. R. Mcneill, Y.-H. Shin, A. S. R. Chesman, *J. Phys. Chem. C* **2019**, *123*, 12062.

[21] W. Chen, J. Zhang, G. Long, Y. Liu, Q. Zhang, *J. Mater. Chem. C* **2015**, *3*, 8219.

[22] L. M. Kozycz, C. Guo, J. G. Manion, A. J. Tilley, A. J. Lough, Y. Li, D. S. Seferos, *J. Mater. Chem. C* **2015**, *3*, 11505.

[23] A. Welford, S. Maniam, E. Gann, L. Thomsen, S. J. Langford, C. R. McNeill, *Org. Electron.* **2018**, *53*, 287.

[24] A. J. Tilley, C. Guo, M. B. Miltenburg, T. B. Schon, H. Yan, Y. Li, D. S. Seferos, *Adv. Funct. Mater.* **2015**, *25*, 3321.

[25] F. S. Etheridge, R. Fernando, J. A. Golen, A. L. Rheingold, G. Sauve, *RSC Adv.* **2015**, *5*, 46534.

[26] I. Welterlich, B. Tieke, *Polym. Chem.* **2013**, *4*, 3755.

[27] H. Zhang, K. Yang, K. Zhang, Z. Zhang, Q. Sun, W. Yang, *Polym. Chem.* **2018**, *9*, 1807.

[28] Z. He, B. Xiao, F. Liu, H. Wu, Y. Yang, S. Xiao, C. Wang, T. P. Russell, Y. Cao, *Nat. Photonics* **2015**, *9*, 174.

[29] P.-L. T. Boudreault, A. Najari, M. Leclerc, *Chem. Mater.* **2011**, *23*, 456.

[30] T. Xu, L. Yu, *Mater. Today* **2014**, *17*, 11.

[31] D. Yang, H. Sasabe, T. Sano, J. Kido, *ACS Energy Lett.* **2017**, *2*, 2021.

[32] Y. Yang, B. Qiu, S. Chen, Q. Zhou, Y. Peng, Z.-G. Zhang, J. Yao, Z. Luo, X. Chen, L. Xue, L. Feng, C. Yang, Y. Li, *J. Mater. Chem. A* **2018**, *6*, 9613.

[33] Y. Li, M. Gu, Z. Pan, B. Zhang, X. Yang, J. Gu, Y. Chen, *J. Mater. Chem. A* **2017**, *5*, 10798.

[34] C. Liang, H. Wang, *Org. Electron.* **2017**, *50*, 443.

[35] J. C. Bijleveld, A. P. Zoombelt, S. G. J. Mathijssen, M. M. Wienk, M. Turbiez, D. M. de Leeuw, R. A. J. Janssen, *J. Am. Chem. Soc.* **2009**, *131*, 16616.

[36] S. Valero, S. Collavini, S. F. Völker, M. Saliba, W. R. Tress, S. M. Zakeeruddin, M. Grätzel, J. L. Delgado, *Macromolecules* **2019**, *52*, 2243.

[37] G.-W. Kim, J. Lee, G. Kang, T. Kim, T. Park, *Adv. Energy Mater.* **2018**, *8*, 1701935.

[38] L. Zhang, C. Liu, J. Zhang, X. Li, C. Cheng, Y. Tian, A. K.-Y. Jen, B. Xu, *Adv. Mater.* **2018**, *30*, 1804028.

[39] B. Zhang, H. Zhang, X. Li, W. Li, P. Sun, W. Yang, *J. Polym. Sci. Part A Polym. Chem.* **2011**, *49*, 3048.

[40] T. Leijtens, I.-K. Ding, T. Giovenzana, J. T. Bloking, M. D. McGehee, A. Sellinger, **2012**.

[41] I. Kang, H.-J. Yun, D. S. Chung, S.-K. Kwon, Y.-H. Kim, *J. Am. Chem. Soc.* **2013**, *135*, 14896.

[42] R. Noriega, J. Rivnay, K. Vandewal, F. P. V. Koch, N. Stingelin, P. Smith, M. F. Toney, A. Salleo, *Nat. Mater.* **2013**, *12*, 1038.

[43] D. Gendron, F. Maasoumi, A. Armin, K. Pattison, P. L. Burn, P. Meredith, E. B. Namdas, B. J. Powell, *RSC Adv.* **2017**, *7*, 10316.

[44] H. Nishimura, N. Ishida, A. Shimazaki, A. Wakamiya, A. Saeki, L. T. Scott, Y. Murata, *J. Am. Chem. Soc.* **2015**, *137*, 15656.

[45] P. Piatkowski, B. Cohen, F. Javier Ramos, M. Di Nunzio, M. K. Nazeeruddin, M. Grätzel, S. Ahmad, A. Douhal, *Phys. Chem. Chem. Phys.* **2015**, *17*, 14674.

[46] H.-S. Kim, C.-R. Lee, J.-H. Im, K.-B. Lee, T. Moehl, A. Marchioro, S.-J. Moon, R. Humphry-Baker, J.-H. Yum, J. E. Moser, M. Grätzel, N.-G. Park, *Sci. Rep.* **2012**, *2*, 591.

[47] S. Makuta, M. Liu, M. Endo, H. Nishimura, A. Wakamiya, Y. Tachibana, *Chem. Commun.* **2016**, *52*.

[48] S. E. Koh, C. Risko, D. A. da Silva Filho, O. Kwon, A. Facchetti, J.-L. Brédas, T. J. Marks, M. A. Ratner, *Adv. Funct. Mater.* **2008**, *18*, 332.

[49] H. Patil, W. X. Zu, A. Gupta, V. Chellappan, A. Bilic, P. Sonar, A. Rananaware, S. V. Bhosale, S. V. Bhosale, *Phys. Chem. Chem. Phys.* **2014**, *16*, 23837.

[50] K. H. Cheon, J. Cho, B. T. Lim, H.-J. Yun, S.-K. Kwon, Y.-H. Kim, D. S. Chung, *RSC Adv.* **2014**, *4*, 35344.

[51] M. Saliba, J.-P. Correa-Baena, C. M. Wolff, M. Stolterfoht, N. Phung, S. Albrecht, D. Neher, A. Abate, *Chem. Mater.* **2018**, *30*, 4193.

[52] S. Yoo, B. Domercq, B. Kippelen, *J. Appl. Phys.* **2005**, *97*, 103706.

[53] N. Wu, Y. Wu, D. Walter, H. Shen, T. Duong, D. Grant, C. Barugkin, X. Fu, J. Peng, T. White, K. Catchpole, K. Weber, *Energy Technol.* **2017**, *5*, 1827.

[54] B. Dänekamp, N. Droseros, D. Tsokkou, V. Brehm, P. P. Boix, M. Sessolo, N. Banerji, H. J. Bolink, *J. Mater. Chem. C* **2019**, *7*, 523.

[55] P. Vivo, A. Ojanperä, J.-H. Smått, S. Sandén, S. G. Hashmi, K. Kaunisto, P. Ihalainen, M. T. Masood, R. Österbacka, P. D. Lund, H. Lemmetyinen, *Org. Electron.* **2017**, *41*, 287.

[56] J. Cao, Y.-M. Liu, X. Jing, J. Yin, J. Li, B. Xu, Y.-Z. Tan, N. Zheng, *J. Am. Chem. Soc.* **2015**, *137*, 10914.

[57] J. Cao, J. Yin, S. Yuan, Y. Zhao, J. Li, N. Zheng, *Nanoscale* **2015**, *7*, 9443.

[58] N. Droseros, B. Dänekamp, D. Tsokkou, P. P. Boix, N. Banerji, *APL Mater.* **2019**, *7*, 041115.

[59] M. Liu, M. Endo, A. Shimazaki, A. Wakamiya, Y. Tachibana, *ACS Appl. Energy Mater.* **2018**, *1*, 3722.

[60] L. Wang, C. McCleese, A. Kovalsky, Y. Zhao, C. Burda, *J. Am. Chem. Soc.* **2014**, *136*, 12205.

[61] M. Liu, M. Endo, A. Shimazaki, A. Wakamiya, Y. Tachibana, *J. Photopolym. Sci. Technol.* **2018**, *31*, 633.

[62] J. S. Manser, P. V. Kamat, *Nat. Photonics* **2014**, *8*, 737.

[63] M. Liu, M. Endo, A. Shimazaki, A. Wakamiya, Y. Tachibana, *J. Photopolym. Sci. Technol.* **2017**, *30*, 577.

[64] G.-W. Kim, G. Kang, J. Kim, G.-Y. Lee, H. Il Kim, L. Pyeon, J. Lee, T. Park, *Energy Environ. Sci.* **2016**, *9*, 2326.

[65] J. Li, L. Wang, X.Yuan, B. Bo, H. Li, J. Zhao, X. Gao *Mater. Res. Bull.* **2018**, *102*, 86.

[66] S. S. Mali, S. K. Desai, S. S. Kalagi, C. A. Betty, P. N. Bhosale, R. S. Devan, Y.-R. R. Ma, P. S. Patil, *Dalt. Trans.* **2012**, *41*, 6130.

Figures

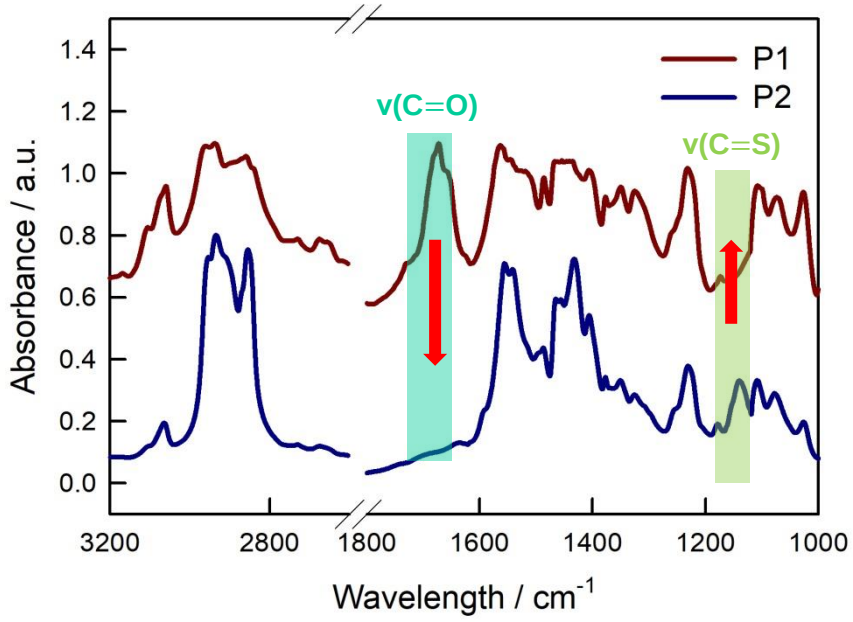

Figure 1. FTIR spectra of KBr dispersions of polymers **P1** and **P2**.

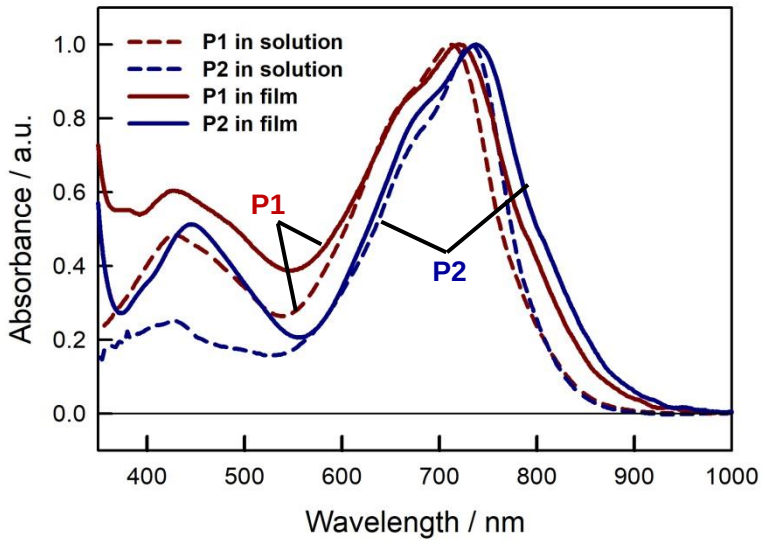

Figure 2. UV/Visible/NIR absorption spectra of **P1** and **P2** in chloroform solution (c=0.05 g/L) and in thin spin-coated films, respectively.

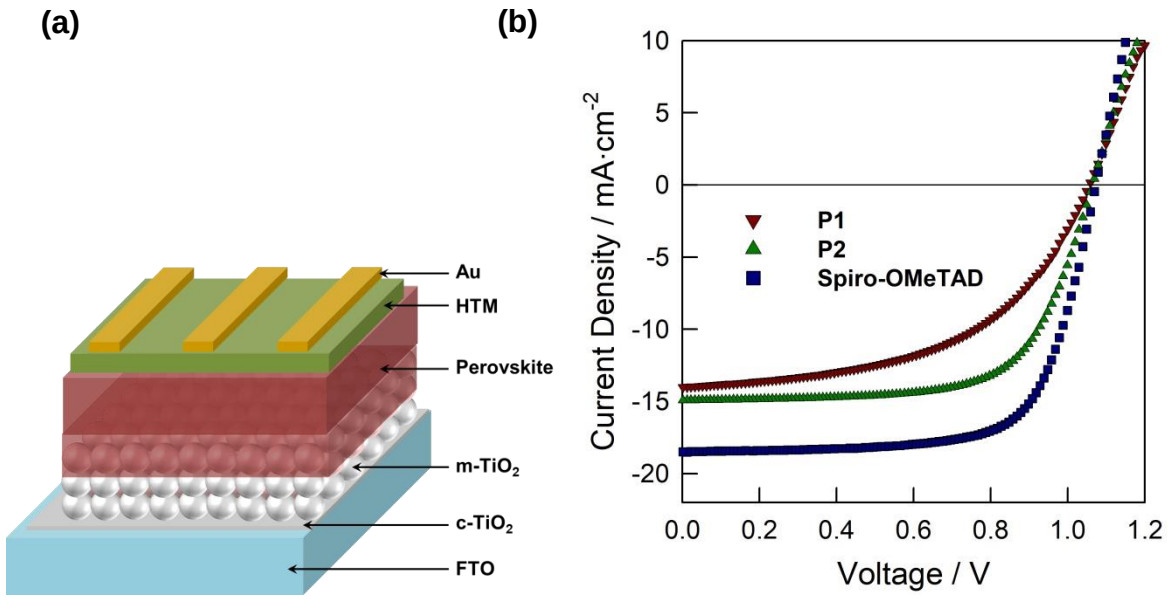

Figure 3. (a) Architecture of the *n-i-p* PSCs studied in this work. As HTM, **P1**, **P2**, and Spiro-OMeTAD have been employed. (b) *J–V* curves (backward sweeps) of the champion PSCs under 1 Sun illumination.

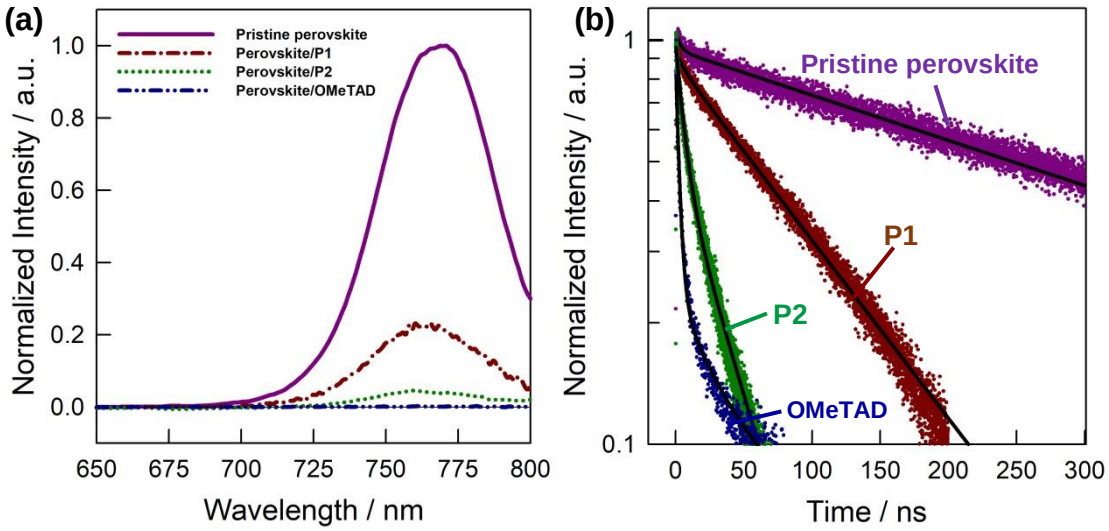

Figure 4. (a) Normalized photoluminescence (PL) spectra of glass/perovskite and glass/perovskite/HTMs, correlated with the number of absorbed photons at excitation wavelength. All samples were excited at 600 nm. (b) Normalized time-correlated single photon counting (TCSPC) decays of glass/perovskite and glass/perovskite/HTMs, excited at 648 nm, and monitored at 765 nm. Solid lines present the fitting results with bi-exponential function $I(t) = A_1 \times e^{(-t/\tau 1)} + A_2 \times e^{(-t/\tau 2)}$.

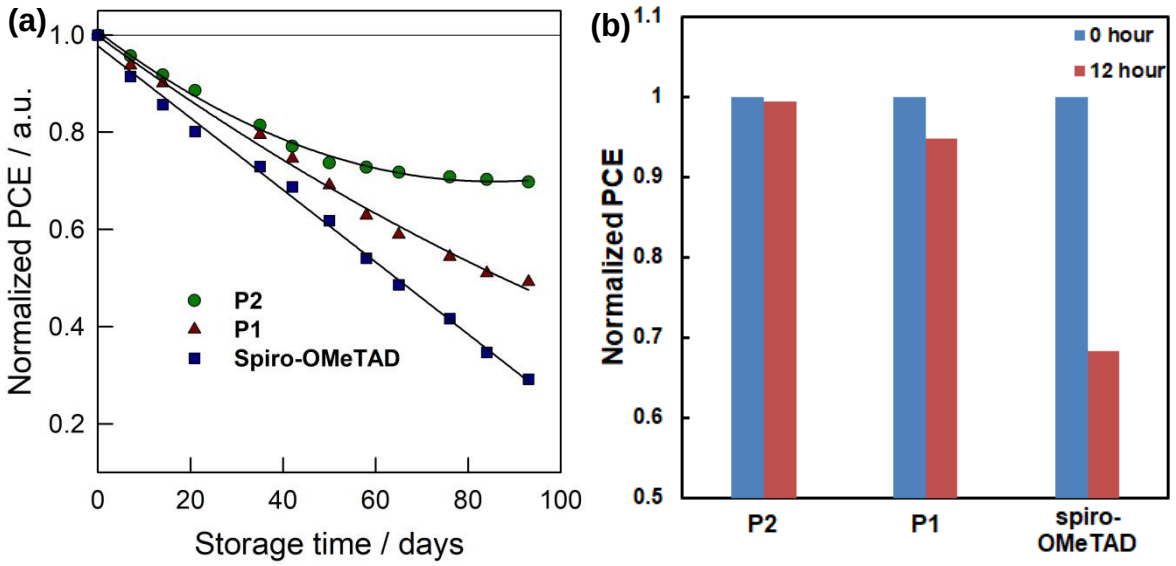

Figure 5. Normalized power conversion efficiencies (PCEs) of PSCs employing different HTMs (**P1**, **P2**, or Spiro-OMeTAD) as a function of (a) shelf-storage time (at 25 ºC and 10% RH) and (b) thermal heating time (at 65 ℃ in nitrogen atmosphere).

Tables

Table 1. Optical and electrochemical properties of **P1** and **P2**.

Compounds	λ_{max} [nm]		$\lambda_{abs,onset}$ of film [nm]	Oxidation onset [V] {HOMO [eV]}	Reduction onset [V] {LUMO [eV]}	$E_g^{opt,a}$/ $E_g^{ec,b}$ [eV]
	in $CHCl_3$	in film				
P1	712	721	875	0.64 {-5.44}	-1.14{-3.66}	1.42/1.78
P2	719	738	865	0.43 {-5.23}	-1.01{-3.79}	1.43/1.44

[a] E_g^{opt} (optical bandgap) was measured at the onset of absorption of polymer film (E_g^{opt} = 1240/$\lambda_{abs,onset}$ eV). [b]E_g^{ec} electrochemical bandgap, HOMO-LUMO gap was calculated according to the equation: $-E_{LUMO} = E_{onset(red)} + 4.8$ eV, and $-E_{HOMO} = E_{onset(ox)} + 4.8$ eV. $E_{onset(ox)}$ and $E_{onset(red)}$ are onset potentials for oxidation and reduction processes *vs*. Fc/Fc^+ couple.

Table 2. Summary of perovskite solar cells performance with different HTMs (The data are from the backward scans).

HTMs	Jsc [mA cm^{-2}]	Voc [V]	FF	PCE [%]	R_S [Ω cm^2]	R_{SH} [kΩ cm^2]
P1	13.6±0.5 (14.2)[a)]	1.04±0.02 (1.06)	0.50±0.02 (0.53)	7.1±0.5 (7.9)	19.04±1.03 (18.01)	0.38±0.15 (0.53)
P2	14.4±0.3 (14.6)	1.04±0.02 (1.06)	0.64±0.01 (0.65)	9.7±0.4 (10.1)	12.80±1.25 (11.55)	3.05±0.30 (3.39)
Undoped spiro-OMeTAD	4.0±0.7 (4.7)	0.77±0.08 (0.86)	0.49±0.04 (0.54)	1.5±0.5 (2.2)	51.33±1.25 (50.08)	0.10±0.05 (0.15)
Doped spiro-OMeTAD	17.5±0.8 (18.5)	1.04±0.03 (1.08)	0.68±0.03 (0.70)	12.3±0.6 (14.1)	8.97±0.46 (8.51)	1.53±0.35 (1.88)

[a)]Values in brackets refer to the photovoltaic parameters of the champion cells.

Table 3. Summary of the fitting results and corresponding dynamic parameters for PL decays of glass/perovskite/HTMs samples.

HTMs	A_1 [%]	τ_1 [ns]	A_2 [%]	τ_2 [ns]	$\tau_{1/e}$ [a)] [ns]	$\tau_{h\text{-}inj}$ [b)] [ns]	$\Phi_{h\text{-}inj}$ [c)] [%]
P1	6.5	7.2	93.5	98.6	87.1	113.8	76.5
P2	51.2	6.5	48.8	38.3	16.9	17.7	95.4
Spiro-OMeTAD	94.4	0.4	5.6	10.6	0.9	0.9	99.3

a) $\tau_{1/e}$ is the effective lifetime of PL decay.
b) $\tau_{h\text{-}inj}$ is the hole injection rate.
c) $\Phi_{h\text{-}inj}$ is the hole injection yield.

Table of contents

Keyword perovskite solar cells

H. Zhang,† M. Liu,† W. Yang, L. Judin, T. Hukka, A. Priimagi, Z. Deng,* P. Vivo*

Thionation enhances the performance of polymeric dopant-free hole-transporting materials for perovskite solar cells

Thionation is a straightforward strategy to dramatically boost the performance of dopant-free polymeric hole-transporting materials (HTMs) for perovskite solar cells. Upon HTM thionation, a nearly 40% enhancement in the power conversion efficiency of the corresponding devices is observed. Such an increase is attributed to the enhancement of both the hole transport within the HTM and the interfacial hole transfer dynamics.